0955-2219(95)00100-X

Mechanical Behaviour of Partially Stabilized Zirconia Crystals with Terbia and Ceria Additives

George A. Gogotsi & Dmitry Yu. Ostrovoy

The Institute for Problems of Strength, National Academy of Sciences of Ukraine,
2 Timiryazevskaya St, 252014 Kiev, Ukraine

Abstract

Mechanical behaviour of partially stabilized zirconia crystals (PSZC) with terbia and ceria additives was investigated under bending and indentation conditions. Test specimens were oriented along the [010] direction and along the axis of crystal growth. The PSZC bending strength (σ_b) was dependent on the crystallographic orientation of the specimens. The specimen volume subjected to stress influenced the PSZC strength. The highest mechanical characteristics were measured for ceria-doped crystals ($\sigma_b = 1.9$ GPa, $K_{1c} = 11.4$ MPa $m^{1/2}$, $E_d = 366$ GPa). The failure process was studied on the Vickers indentation, with special emphasis put on the development and propagation of lateral cracks. Anisotropy of lateral cracks in the (100) plane associated with that of the elastic moduli was revealed. At the same time anisotropy of radial cracks and hardness was not found. A new version of the equation to evaluate the fracture toughness (K_c^v) on the Vickers indentation was derived. The K_c^v values calculated by this equation correspond to those (K_{1c}) obtained by an SENB method.

1 Introduction

Considerable attention has recently been focused on partially stabilized zirconia crystals (PSZC),[1-3] some properties of which meet the requirements placed on structural materials. This rather high level of interest is probably also caused by technology[4] which allows the production of materials of high strength and fracture toughness. In published works e.g. Refs 3, 5 and 6, the authors mainly cited data on PSZC containing only yttria as a major additive (Y–PSZC). For testing, different, often contradictory procedures were used[3,7,8] with primary emphasis put on the physical nature of processes determining strength and deformation of these crystals[3,5]. It was shown[9,10] that other oxides of rare earth elements (ytterbium, cerium, etc.) present in Y–PSZC can also exert a positive influence not only on the process to make these crystals, but also on their physico mechanical characteristics. However, despite these data, certain problems associated, e.g. with the anisotropy of Y–PSZC properties still remain poorly investigated. Several results have been obtained[11,12] for the hardness of such crystals or for the development of cracks in them; however, detailed investigations of lateral cracks with the account of their crystallographic orientation have not been performed. As opposed to radial cracks, the latter can be of importance for such Y–PSZC applications as cutting elements of surgical instruments, bearing components, etc.[4,9] the production of which is accompanied with different machining, including abrasive.

The present work is therefore devoted to a complex investigation of mechanical properties of Y–PSZC containing terbia and ceria additives, with special emphasis on the development of lateral cracks in relation to other mechanical characteristics. This work continues our studies on zirconia crystals started in Refs 9 and 10.

2 Experimental Procedures

Partially stabilized zirconia single crystals with 3 mol% yttria and containing 0.3 mol% terbia (Y–Tb–PSZC) and 0.3 mol% ceria (Y–Ce–PSZC) were chosen for the investigations. These crystals, like those studied previously,[10] were prepared by direct high-frequency scull-melting technique at the Institute of General Physics, Russian Academy of Sciences.

Rectangular test specimens were cut from crystalline blocks with a diamond saw, their surfaces were ground and sharp edges rounded. The longitudinal axis of some specimens (Y–Tb–PSZC-A and Y–Ce–PSZC) was oriented by the Laue

back reflection method along the [010] direction, their mutually perpendicular surfaces corresponded to the {100} planes. The longitudinal axis of Y–Tb–PSZC-B specimens was approximately directed along the axis of crystal growth and was not strictly related to one of the characteristic directions in the cubic lattice,[13] i.e. the specimens were oriented in the same manner as for studying similar materials in Ref. 14.

Bending tests, as in Refs 4 and 9, were performed by our procedures.[15] All the specimens had the same cross-section (3·5 × 5·0 mm), the length of Y–Tb–PSZC-A specimens was about 25 mm, while the specimens of other crystals were about 45 mm long. The difference was determined by the dimensions of crystalline blocks. Therefore, the specimens were tested by three- and four-point bending. In the first case the span between supporting rollers was 20 (or 10) mm, in the second case it was 40 and 20 mm. Using different bending configurations, one could also evaluate a possible influence of the specimen volume subject to stress on the strength of the crystals under study.

In three-point bending tests the well known fact from applied mechanics was taken into account, viz. the plane stress state of the specimens occurring on such loading. Additional deflection of the specimens because of shear stresses can affect the magnitude of elastic moduli.[16] It is interesting that this fact is not usually taken into account during investigation of ceramics and single crystals. In this work we performed corrections of the experimental data obtained under three-point bending using the equation:[16]

$$E_{st} = \frac{L^3}{48J}\left[1+3\left(1+\nu\right)\left(\frac{h}{L}\right)^2\right]\frac{P}{\delta}, \quad (1)$$

where E_{st} is the static elastic modulus on bending, P is the load, δ is the deflection, J is the moment of inertia of the cross-section, ν is Poisson's ratio, L is the span between supporting rollers and h is the height of a specimen.

Poisson's ratios (ν) were calculated from the data obtained on uniaxial compression of specimens. In this case lateral and longitudinal strain components were measured by resistance strain gauges glued to the specimen surfaces. These strain components were used to calculate known Poisson's ratio. Dynamic elastic moduli (E_d) were determined, as previously,[9,10] from longitudinal ultrasonic velocity data, v_1, measurements ($E_d = \rho v^2_1$, where ρ is the density of the material). It should be noted that here we used the concepts 'dynamic' and 'static' elastic moduli, though, as applied to crystals, one should speak rather about elastic constants for one or other crystallographic direction.[6,13] Thus, in our further discussions we con-

fined ourselves to the above terminology which is widely used in engineering practice and can considerably simplify the analysis of the data.

The bending strength (σ_b) was calculated by applied mechanics known relations ($\sigma_b=2aP/bh^2$, where a is the length of a cantilever part of a specimen and b is the width of a specimen). As in Refs 9 and 10, a well known SENB method[17] was used to determine fracture toughness characteristics, e.g. the critical stress intensity factor (K_{1c}). The specimens were notched on their narrower surface (3·5 mm) over a half-height of their cross-section (2·5 mm) and placed with the same surface on the supporting rollers having a 20 mm span. The K_{1c} values were determined by the equation: $K_{1c} = \sigma_b c_n^{0·5} Y$, where c_n is the length of the notch and Y is the geometric factor determined from the tables.[17] The crack propagation in crystal specimens was studied by the traditional Vickers method. The data obtained were also used to evaluate the fracture toughness (K_c^v) of the crystals (see below).
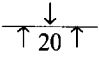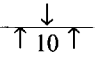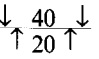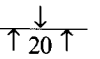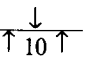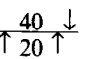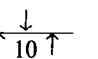
3 Results

3.1 Bending strength, elasticity and fracture toughness

Major tests were performed on Y–Tb–PSZC-A specimens, the data on other crystals were used for comparison.

Strength characteristics were determined in the following way. The Y–TB–PSZC-A specimens were tested only by three-point bending, Y–Tb–PSZC-B and Y–Ce-PSZC were first tested by four-point bending, then by three-point (Table 1). The strength values (σ_b) of all studied specimens varied depending on the bending configuration. Thus, with a smaller span between supporting rollers, σ_b for the Y–Tb–PSZC-B and Y–Ce-PSZC specimens tends to increase (Table 1). The σ_b values of the Y–Tb–PSZC-A specimens were somewhat lower under such loading conditions. Maximum σ_b values (for several specimens, e.g. Y–Ce-PSZC they reached 1·9 GPa) corresponded to the highest values of elastic moduli (Table 2) for the [010] direction.

It is interesting to note that the differences were also observed in the nature of fracture surfaces for all specimens after bending tests. The Y–Tb–PSZC-A and Y–Ce-PSZC specimens exhibited traces of secondary cracking on their fracture surfaces visible even to the naked eye (Fig. 1(a)), while the fracture surface of Y–Tb–PSZC-B was smoother, displaying smaller flake-like cleavage. All the specimens (see also Ref. 9) are characterized by a step-wise propagation of the main crack

Table 1. Average bending strength of crystals

	Material						
	Y–Tb–PSZC-A			Y–Tb–PSZC-B		Y–Ce–PSZC	
Bending configuration[a]	↓ 20	↓ 10	↓ 40 ↓ 20	↓ 20	↓ 10	↓ 40 ↓ 20	↓ 10
Bending strength(MPA)	1611	1197	416	630	853	1378	1698

[a]The figures give the span between supporting rollers (mm).

Table 2. Average physical characteristics of crystals

Material	Density (g/cm^3)	Ultrasonic velosity(m/s)	Elastic moduli (GPa)	
			Dynamic	Static
Y–Tb–PSZC-A	6·06	7630	352	307[a] (334[b])
Y–Tb–PSZC-B	6·06	5399	177	166[c]
Y–CE–PSZC	6·07	7769	366	369[c]

[a]Three-point bending.
[b]Values corrected by eqn (1).
[c]Four-point bending.

front (Fig.1(b)). Fracture sources were concentrated in the surface layer on the side of a tensile zone, however we did not succeed in establishing their type because of the complex structure of fracture surfaces.

Bending tests of SENB specimens enabled K_{1c} values to be calculated, they were 9·96, 7·0 and 11·43 MPa m$^{1/2}$ on average for Y–TB–PSZC-A, Y–Tb–PSZC-B and Y–Ce–PSZC, respectively. In the first and third cases notch directions were coincident with [001].
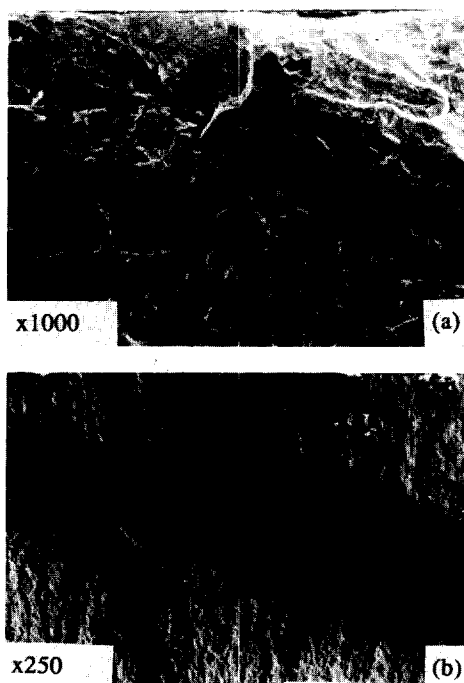

Fig. 1. (a) Fracture patterns of Y–Tb–PSZC-A specimens: flake-like surface cleavage, (b) step-wise propagation of the main crack front.

3.2 Vickers indentation tests

3.2.1 Indentation surfaces

Both groups of Y–TB–PSZC specimens were indented in the loading range of 0·1–200 N, since a further increase of loads resulted in less satisfactory impressions. The Y–Ce–PSZC specimens were also tested at higher loads (up to 300 N), since this problem arose to a less extent. The Vickers indenter was successively rotated through 360°C relative to the longitudinal axis of the specimen in a chosen plane only for Y–Tb–PSZC-A specimens, in the case of other crystals it was rotated only through 90°.

For all crystals, hardness values (H_v) determined from the impression half-diagonal[18] did not practically depend on the indentation direction in the planes under investigation (Fig. 2). In this case an increase in loading up to 70 N resulted in a certain decrease of H_v, e.g. for Y–Tb–PSZC-A from 14·3 GPa at 0·2 N to 12·5 GPa at 70 N. Starting from this load, H_v remained practically constant (this problem was detailed in Ref. 10).

In the process of indentation the cracks of different types were formed, viz. radial (Palmqvist)[10,19] and lateral,[10,20] or both. The presence of radial cracks is confirmed by the fact that partial grinding-off of the impressions resulted in the separation of such cracks from each corner of the impression (see also Refs 9 and 10). The extent of radial cracking was evaluated by an average length $[\bar{l} = \frac{1}{4}(l_1 + l_2 + l_3 + l_4)]$ of these cracks measured from each corner of the impression (Fig. 3). A relative size of lateral cracks was characterized by the parameter L $(\bar{R}) = \frac{ON-OM}{OM} \approx \frac{R}{0.707a} - 1$ (Fig. 3), where $\overline{ON} = \bar{R}$ is the average distance from the impression center to the most distant part of the
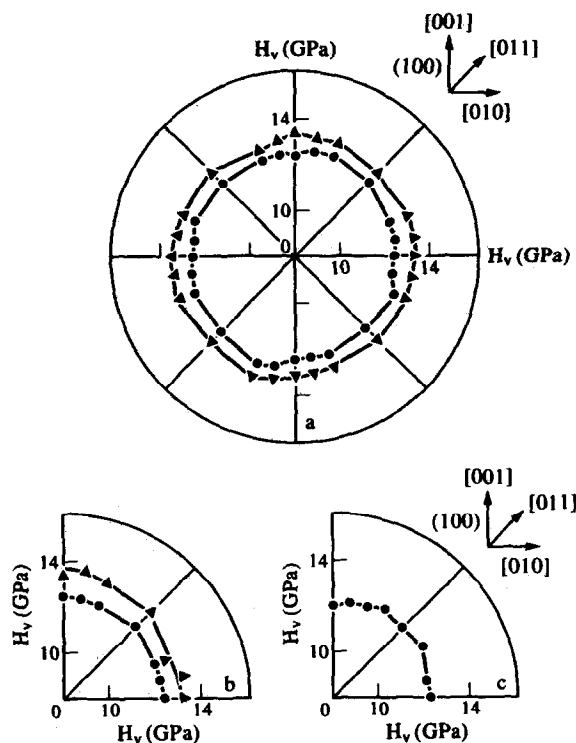
Fig. 2. Hardness (H_v) versus an angle of indenter rotation for: (a) Y–Tb–PSZC-A, (b) Y–Tb–PSZC-B, (c) Y–Ce–PSZC. Loads: 50 N (▲) and 100 N (●).

Fig. 4. Average length of radial cracks ($\bar{l}$) versus an angle of indenter rotation for (a) Y–Tb–PSZC-A, (b) Y–Tb–PSZC-B and (c) Y–Ce–PSZC. Loads: 50 N (▲) and 100 N (●).

front of the lateral crack calculated from each side of the impression, OM is the half-length of the impression side ($OM = a \sin 45°$) and a is the half-diagonal of the impression.

The experiments have demonstrated that the value of $\bar{l}$ for all crystals varies slightly depending on the indentation direction (Fig. 4). This may be investigated by drawing regression curves through a series of experimental points (Fig. 4). It was necessary to use this approach since experimental points had a relatively wide scatter in different directions. At the same time the extent of lateral cracking L ($\bar{R}$) differed considerably for the planes under consideration. Thus, when the indenter is turned in the (100) plane (Y–Tb–PSZC-A and Y–Ce–PSZC specimens), L ($\bar{R}$) varied from a certain maximum value ([010] direction) at a given
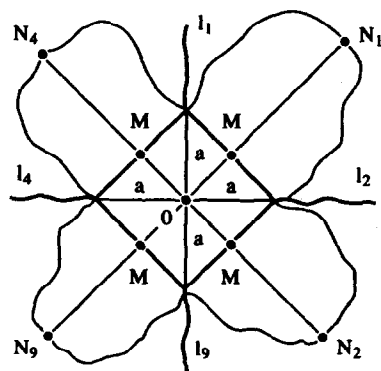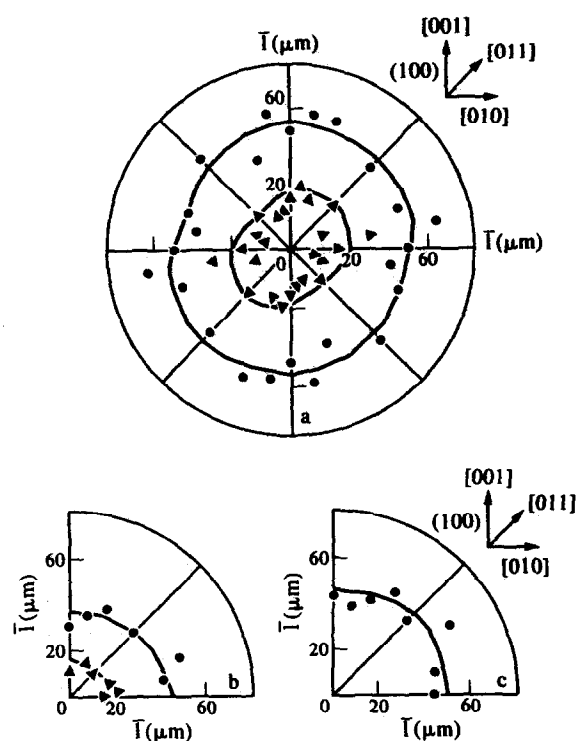
load to a minimum one ([011] direction) and so on. If we average the data obtained (as in Fig. 4), they can graphically be represented as four–fold symmetry (Fig. 5(a),(c)). In this case $L(\bar{R})$ for Y–Ce–PSZC were lower (Fig. 5(c)) than those for Y–Tb–PSZC-A (Fig. 5(a)) at the same loads. For Y–Tb–PSZC-B

Fig. 3. Schematic representation of cracks formed around the Vickers impression (explanations in the text).
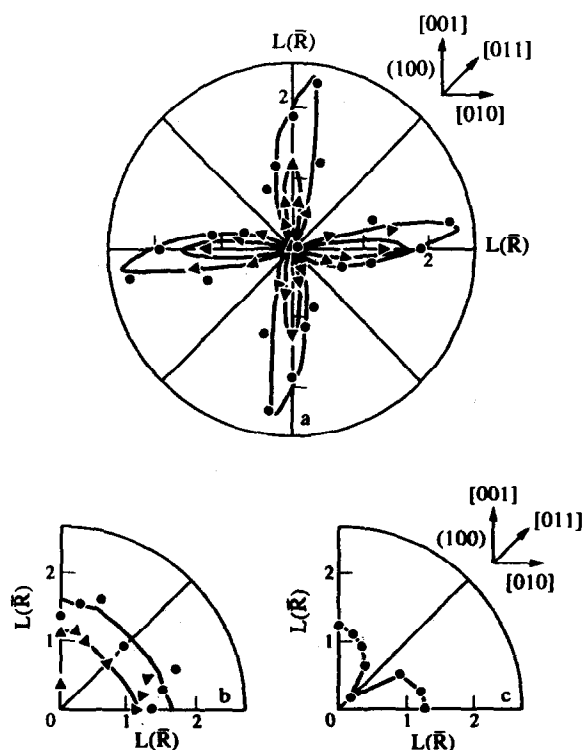

Fig. 5. Relative length of lateral cracks $L(\bar{R})$ versus an angle of indenter rotation for (a) Y–Tb–PSZC-A, (b) Y–Tb–PSZC-B and (c) Y–Ce–PSZC. Loads: 50 N (▲) and 100 N (●).

specimens $L(\bar{R})$ did not depend on the indentation direction, and its absolute values were somewhat different for different specimen surfaces (one of them is shown in Fig. 5(b)).

3.2.2 Fracture toughness

On the basis of earlier investigations,[9,21] we made the next step in terms of evaluating the fracture toughness of zirconia crystals from the length of radial cracks. For this purpose we used experimental values of a and $\bar{l}$ at various loads to plot calibration curves for each crystal[19] as a relation between normalized fracture toughness and normalized length of radial cracks. All these curves were approximated using an equation of the following type[22]

$$\frac{K_c^v \phi}{H_v a^{0.5}} \left(\frac{H_v}{E\phi}\right)^{0.4} = M \left(\frac{c}{a}\right)^{-N} . \quad (2)$$

In this equation the left side is the normalized fracture toughness, ϕ is the constraint factor ($\phi \approx 3$), H_v is the load-independent hardness and E is the static or dynamic elastic modulus. The right side contains the normalized length of radial cracks [$\frac{c}{a} = \frac{l+a}{a}$] and the coefficients ($M$ and N) are determined experimentally. In this case $c = l+a$ was taken as the length of radial cracks instead of ι (Fig. 4) which is often used in practice.[10,18,21] The value of K_c^v, as in Ref. 18, was set equal to K_{1c} and $H_v = 12.5$ GPa was chosen as its average value for all crystals in a load-independent regime. Major parameters of calibration curves in Fig. 6 being a log–log plot determined by the least-squares method are summarized in Table 3. The values of K_c^v calculated from these data, e.g. for Y–Tb–PSZC-A (Fig. 8), did not differ significantly from those obtained by the SENB method. Such calculations should also account for possible variations of elastic modulus (E) in different crystallographic directions.
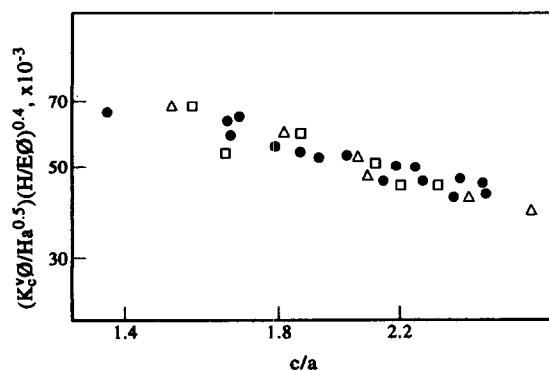
We established that at least for Y–Tb–PSZC-A,

Table 3. M and N coefficients in eqn (2)

Material	Coefficient		Correlation coefficient
	M	*N*	
Y–Tb–PSZC-A	0·092	0·80	0·96
Y–Tb–PSZC-B	0·099	0·92	0·99
Y–Ce–PSZC	0·097	0·90	0·89

different E values, all other coefficients in the left side of eqn. (2) being constant, contributed only to M changes. At the same time the relations between a and c, e.g. in the [010] and [011] directions, were practically identical (equal values of N) despite a different extent of lateral cracking. The M and E values are inversely proportional, as a result we have practically coincident K_c^v values for a number of M and E values. Therefore, in our case the calculations were restricted to the M values (Table 3) corresponding to the E values obtained in the present work.

4 Discussion

The results obtained show that relatively high strength values correspond at least to the [010] direction in the (100) plane. This was already recognised.[9] By and large one may say that for such crystals, high strength values σ_b correspond to higher elastic moduli (Tables 1 and 2).

It should be noted that, for polished Y–PSZC specimens which contained only Y_2O_3, a σ_b of 2 GPa was found[2]. Among the crystals under investigation only some Y–Ce–PSZC specimens exhibited similar values of σ_b (~1.9 GPa), and the state of the specimen surface (ground or polished) for all crystals did not exert a noticeable influence on the magnitude of σ_b. This indicates that the strength of such crystals is probably determined

Fig. 6. Normalized fracture toughness versus normalized length of radial cracks for Y–Tb–PSZC-A (●), Y–Tb–PSZC-B (△) and Y–Ce–PSZC (□).
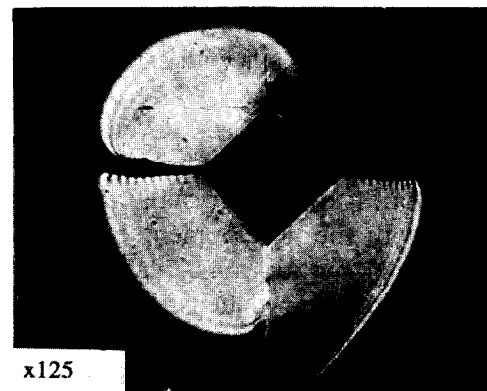

Fig. 7. Lateral and radial cracks around the impression on the Y–Ce–PSZC-A specimen surface corresponding (100) plane at a 150 N loading (the diagonals of the impression coincide with [010] and [001] directions).

rather by structural features in the bulk of the material rather than the surface effects. A reduction of σ_b for Y–Tb–PSZC-A specimens (Table 1) on three-point bending (10 mm span) could also be associated with the latter. Although for the specimens of other crystals a growth of σ_b was observed under the same loading conditions, which does not contradict Weibull's theory of strength.[23] Lower σ_b values for Y–Tb–PSZC-A specimens were not explained convincingly enough. However, such regularity is confirmed by testing of these specimens under different conditions.

Y–Tb–PSZC-A and Y–Ce–PSZC specimens exhibited the highest elastic moduli (Table 2). They are quite close to the literature data[6] for specimens of these crystals having similar orientation. The elastic moduli Y–Tb–PSZC-B specimens were much lower (Table 2). As was expected,[16] the static elastic moduli, E_{st}, determined for Y–Tb–PSZC-A specimens on their three-point bending, as in Ref. 9, were lower than the dynamic moduli E_d (Table 2). It is interesting that the uniaxial compression of these specimens in the [010] direction resulted in an elastic modulus of 370 GPa which slightly differed from E_d. The calculated Poisson's ratio (ν) was 0·17. It does not contradict[24] the values of ν for ceramics and related crystals which are usually in the range of 0·13–0·32. As a rule, materials with high elastic moduli exhibit lower ν. The value of E_{st} corrected by eqn. (1) was 334 GPa. For the specimens of other crystals this procedure was not necessary, since they were tested on four-point bending. A certain discrepancy between E_d and E_{st} for Y–Tb–PSZC-B obtained under the same loading conditions is probably associated with the fact that the specimen surfaces correspond to different crystallographic planes.

It should be noted that elastic moduli for Y–Tb–PSZC were measured on specimens cut from different crystalline blocks. However, they point to a considerable anisotropy of elastic properties of such crystals since all crystals were grown under similar conditions.

From the analysis of crack development around the impressions, it can be concluded that lateral cracks appearing in the crystals are not directly connected with the development of radial cracks. It is confirmed by additional data obtained, e.g. for Y–Tb–PSZC-A specimens. For them, depending on the indentation direction in the (100) plane, different sequence of crack types was observed. Thus, for the impressions where the diagonal is parallel to [010], a threshold value of the load (P_r) when first radial cracks appeared from the corners of the impression was 20 N. For the [011] direc-

tion P_r is equal to 15 N. Lateral cracks around the impressions when their diagonals were oriented along [010] were observed at a load (P_L) of 2 N, i.e. long before the radial ones appeared. The same was observed for Y–PSZC.[21] In the [011] direction the picture was quite opposite: radial cracks preceded the lateral ones. The latter were observed only at P_L=40–50 N. The Y–Ce–PSZC specimens in the [010] direction exhibited P_r=50 N and P_L=10 N. We could not establish certain specific P_r and P_L for Y–Tb–PSZC-B specimens since their surfaces displayed quite different fracture patterns. It should be noted that in Ref. 10 most equal values of P_L but higher values of P_r were observed for similar crystals in the same planes. This is probably caused by the fact that the tests in Ref. 10 were performed at loads of 50 N or higher as well as by the fact that, in the two cases, optical microscopes with different resolution levels were used.

For Y–Tb–PSZC-A and Y–Ce–PSZC the chipping around the impressions with the diagonals oriented along the [010] direction occurred starting from 70 and 200 N, respectively. This phenomenon is due to the uplift on the front of lateral cracks. These chips were observed in the [011] direction, e.g. for Y–Tb–PSZC-A already at 100 N or higher, whilst for Y–Tb–PSZC-B this value was not established because of a considerable scatter of experimental data for arbitrarily chosen directions.

Thus, the results show that in many cases radial cracks in these crystals play the role of a barrier for the propagation of the front of lateral cracks to an adjacent sector of the impression (Fig. 7), this was also observed for ceramics.[20] Radial cracks do not influence the distance of the front of lateral cracks from the center of an impression (ON in Fig. 3) for various loads and directions which also points to the absence of relationship between these types of cracks. For comparison, fully stabilized zirconia crystals (FSZC) exhibited[25] longer radial cracks in [110] as compared to [100] in the (100) plane. It was considered to be associated with the influence of lateral cracks. The latter were of minimum sizes in the [110] direction. Such influence is sometimes explained[20] by the redistribution of strain energy in favour of radial cracks due to a smaller extent of lateral cracking. As was shown above, we did not observe any noticeable anisotropy of radial cracking (Fig. 4) and, as a result, of the fracture toughness (see also [10]). Even when we increased the number of impressions up to 15, e.g. on the (100) surface of Y–Tb–PSZC-A specimens, 100 N loads give l values of 60 μm for [010] ($L(\bar{R})$=2) and of 72 μm for [011] ($L(\bar{R})$=0·19) which is within the scatter of

experimental data. It also applies to the hardness of such crystals (earlier noticed for Y–PSZC[12]), while FSZC displayed[26] its strong anisotropy in the (100) plane. The graphic representation of this anisotropy resembles the variation of elastic moduli[6] and $L(\bar{R})$ (in our case) (Fig. 5) in the same crystallographic planes. One may say that for Y–Tb–PSZC-A and Y–Ce–PSZC the anisotropy of lateral cracks is proportional to that of the elastic moduli: the higher $E_{st}(E_d)$, the higher $L(\bar{R})$. It is interesting that the same relationship was established[27] for several cubic ionic crystals but only between the anisotropy of elastic modulus and that of hardness.

We should also emphasize particular behaviour of crystals on indentation as the formation of 'irregular' radial cracks around some impressions (see also Refs 10,14), these cracks propagate from the sides of the impression or at an angle from its corners. Such cracks are the most characteristic of the impressions, the diagonals of which are oriented along [011]. We did not take them into account when the fracture toughness of crystals was evaluated.

To calculate fracture toughness (K_c^y) from the length of radial cracks, quite a number of semiempirical relations have been proposed,[18,19,22] based on the models of half-penny or Palmqvist cracks. The application of several well known and widely used equations[18]

$$K_c^y = 0.028 \; H_v a^{0.5} \left(\frac{E}{H_v}\right)^{0.5} \left(\frac{c}{a}\right)^{-1.5}, \tag{3}$$

$$K_c^y = 0.142 \; \frac{H_v a^{0.5}}{\phi} \left(\frac{E\phi}{H_v}\right)^{0.4} \left(\frac{c}{a}\right)^{-1.56} \tag{4}$$

and

$$K_c^y = 0.035 \; \frac{H_v a^{0.5}}{\phi} \left(\frac{E\phi}{H_v}\right)^{0.4} \left(\frac{c}{a} - 1\right)^{-0.5}. \tag{5}$$
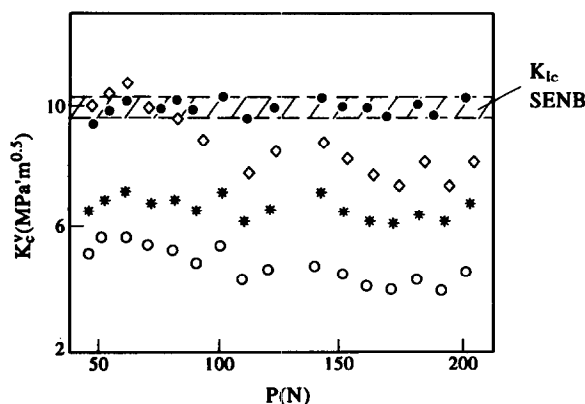

Fig. 8. Fracture toughness (K_c^y) versus the indentation load (P) for Y–Tb–PSZC-A determined by eqn (2) (●), eqn (3) (○), eqn (4) (◇) and eqn (5) (∗).

To evaluate fracture toughness, e.g. of Y–Tb–PSZC-A crystals, resulted (Fig. 8, see also Ref. 10) in K_c^y values which are lower than those obtained by a conventional (SENB) method. It can point to the differences in propagation of radial cracks in ceramics (eqns (3)–(5) were proposed for the latter) and in the crystals under study. Therefore, numerical coefficients from Table 3 substituted in eqn (2) which is similar to eqns (3)–(5) in its structure are more suitable for practical calculations of K_c^y. These coefficients characterize a real behaviour of such crystals on indentation. The equation derived in Ref. 21 which was used[10] to evaluate K_c^y of similar crystals contained coefficients somewhat different in their magnitude. Therefore, it should probably be considered as a foregoing approximation of the problem to be solved. The fact that calibration curves (Fig. 6, Table 3) are spaced so closely is most likely to be random in nature. A relative position of these curves can be different for the specimens of other crystals taking into account possible anisotropy of their mechanical characteristics.

5 Conclusions

The complex investigation of zirconia crystals stabilized with yttria and containing terbia and ceria additives gave additional information about the mechanical behaviour of these materials. It further elucidated the poorly studied field of lateral cracking of crystals on Vickers indentation. This information is also of great interest for the application of crystals as a material for surgical instruments,[9] since this lateral cracking resembles fracture features observed on the surface of scalpels during their sharpening. It gives the impression that the performance of these crystals at room temperature applications can be inferior to that of similar ceramics. It is associated with noticeable local failure when in contact with a sharp concentrator (some grains of abrasive powder, etc.). This behaviour of the crystals was not specially treated by earlier investigators.

In addition, the data obtained in the present work could be useful for the development of more perfect crystals possessing more uniform structure (data on fractographic investigations were published previously[9,10]). The results (including the equation for determining K_c^y) suggest that we should concentrate on the development of the most acceptable approaches for evaluating the fracture toughness of crystals. This problem should be given as much attention as that paid to advanced technical ceramics (see, e.g., Ref. 28).

Acknowledgements

References

1. Ingel, R. P. & Rice, R. W., Room-temperature strength and fracture of ZrO_2-Y_2O_3 single crystals. *J. Am. Ceram. Soc.*, **65** (1982) C.108–9.
2. Ingel, R. P., Lewis, D., Bender, B. A. & Rice, R. W., Physical, microstructural and thermomechanical properties of ZrO_2 single crystals. In *Advances in Ceramics*, Vol. 12, *Science and Technology of Zirconia II*, eds N. Clausen, M. Ruhle & A. H. Heuer. American Ceramic Society, Columbus (1984) 408–14.
3. Heuer, A. H., Lanteri, V. & Dominguez-Rodriguez, A., High-temperature precipitation hardening of Y_2O_3 partially-stabilized ZrO_2 (Y–PSZ) single crystals. *Acta Metall.*, **37** (1989) 559–67.
4. Gogotsi, G. A., Lomonova, E. E. & Osiko, V. V., Studies of mechanical characteristics of zirconia single crystals for structural application. *Refractories*, **32** (1991) 14–7 (Transl. from Russian).
5. Lankford, J., Page, R. A. & Rabenberg, L., Deformation mechanism in yttria-stabilized zirconia. *J. Mater. Sci.*, **23** (1988) 4144–56.
6. Ingel, R. P. & Lewis, D., Elastic anisotropy in zirconia single crystals. *J. Am. Ceram. Soc.*, **71** (1980) 265–71.
7. Dominguez-Rodriguez, A., Lanteri, V. & Heuer, A. H., High-temperature precipitation hardening of two-phase Y_2O_3-partially-stabilized ZrO_2 single crystals: a first report. *J. Am. Ceram. Soc.*, **69** (1986) 285–7.
8. Lankford, J., Inverse strain rate effects and microplasticity in zirconia crystals. *J. Mater. Sci. Lett.*, **8** (1989) 947–9.
9. Gogotsi, G. A., Lomonova, E. E. & Pejchev, V. G., Strength and fracture toughness of zirconia crystals. *J. Eur. Ceram. Soc.*, **11** (1993) 123–32.
10. Gogotsi, G. A., Dub, S. N., Lomonova, E. E. & Ozersky, B. I., Vickers and Knoop indentation behaviour of cubic and partially stabilized zirconia crystals. *J. Eur. Ceram. Soc.*, **15** (1995) 405–13.
11. Martinez-Fernandez, J., Jimenez-Melendo, M., Dominguez-Rodriguez, A. & Heuer, A. H. Elevated temperature studies of microindentation of Y-PSZ. In *Proceedings of the 11th Risø International Symposium on Metallurgy and Materials Sciences: Structural Ceramics-Prossesing, Microstructure and Properties.* eds J. J. Bentzen *et al.* Risø National Laboratory, Roskilde, Denmark (1990) 413–8.
12. Saiki, A., Ishizawa, N., Mitsutani, N. & Kato, M., SEM observation of the stress-induced transformation by Vickers indentation in Y-PSZ crystals. *J. Ceram. Soc. Jpn. Int. Edn.*, **97** (1989) 41–6.
13. Ingel, R. P., Lewis, D., Errors in elastic constant measurements in single crystals. *J. Am. Ceram. Soc.*, **71** (1988) 261–4.
14. Gogotsi, G. A., Galenko, V. I., Ozersky, B. I., Lomonova, E. E., Myzina, V. A., Vishnyakova, M. A. & Kalabukchova, V. E., Strength and fracture toughness of yttria and terbia-doped zirconia crystals. *Refractories*, **34** (1993) 303–12 (Transl. from Russian).
15. Gogotsi, G. A., Test method of advanced ceramics, reasonable approaches for standardization of ceramics. *Key Engng. Mater.*, **56–57** (1991) 419–34.
16. Timoshenko, S. P., Strength and vibration of structural elements. *Nauka, Moscow*, (1975) 704 (in Russian).
17. Brown, W. F. & Srawley, J. E., Plane strain crack toughness testing of high strength metallic materials. ASTM STP 410. *Am. Soc. Test. Mater.*, (1967) 13–15.
18. Li, Z., Ghosh, A., Kobayashi, A. S. & Bradt, R. C., Indentation fracture toughness of sintered silicon carbide in the Palmqvist crack regime. *J. Am. Ceram. Soc.*, **72** (1989) 904–11.
19. Lankford, J., Indentation microstructure in the Palmqvist crack regime: implications for fracture toughness evaluation by the indentation method. *J. Mater. Sci. Lett.*, **1** (1982) 493–5.
20. Cook, R. F., Pascucci, M. R. & Phodes, W. H., Lateral cracks and microstructural effects in the indentation fracture of yttria. *J. Am. Ceram. Soc.*, **73** (1990) 1873–8.
21. Dub., S. N. & Gogotsi, G. A., Indentation fracture toughness of zirconia crystals. *J. Aust. Ceram. Soc.*, (in press).
22. Evans, A. G. & Charles, E. A., Fracture toughness determinations by indentation. *J. Am. Ceram. Soc.*, **59** (1976) 371–2.
23. Weibull, W., A statistical distribution function of wide applicatibility. *J. Appl. Mech.*, **18** (1951) 293–7.
24. French, S. S. J., Ceramics in reciprocating internal combustion engines. *SAE Techn. Pap. Ser.*, N841135 (1984) 14.
25. Pajares, A., Guiberteau, F., Dominguez-Rodriguez, A. & Heuer, A. H., Indentation-induced cracks and the toughness anisotropy of 9·4 mol%yttria-stabilized cubic zirconia single crystals. *J. Am. Ceram. Soc.*, **74** (1991) 859–91.
26. Pajares, A., Guiberteau, F., Dominguez-Rodriguez, A. & Heuer, A. H. Microhardness and fracture toughness anisotropy in cubic zirconium oxide single crystals. *J. Am. Ceram. Soc.*, **71** (1988) 332–3.
27. Sirdeshmukh, D. B. & Kishen Rao, K., Hardness anisotropy in cubic ionic crystals. *J. Mater. Sci. Lett.*, **7** (1988) 567–8.
28. Quinn, D. G., Salem, Y., Bar-en, Y., Cho, K., Foley, M. & Fang, H. Fracture toughness of advanced ceramics at room temperature. *J. Res. Natl Inst. Standards Technol.*, **97** (1992) 579–607.